JOURNAL OF CATALYSIS 3, 341–352 (1964)

Gas Diffusion in Porous Catalysts. Diffusion-Controlled Elution of Physically Adsorbed Hydrocarbons

R. L. GORRING AND A. J. DEROSSET

From the Universal Oil Products Company, Des Plaines, Illinois

Received January 9, 1964

A technique has been developed for the experimental determination of the effective diffusivity of porous catalyst materials. Results obtained by eluting gaseous hydrocarbons from five spherical aluminosilicate materials support the theory of diffusion accompanied by rapid desorption. The method is shown to be applicable to determination of the average diffusivity of a catalyst batch from a single experiment. It is shown that where adsorption is a relatively important factor, such as in the system silica-isobutane, surface diffusion accounts for the major part of mass transport in the pores.

INTRODUCTION

The over-all process of chemical transformation on porous catalytic materials involves a definite number of steps linked in series. These are:

1. Diffusion of reactants to the gross exterior of the catalyst granule.
2. Diffusion of reactants through the porous matrix to the reactive surface.
3. Adsorption of reactants.
4. Reaction.
5. Desorption of products.
6. Diffusion of products through the porous matrix to the exterior surface.
7. Diffusion of reactants away from the exterior surface and into the fluid surrounding the granule.

The particular conditions of reaction determine which of these steps is rate-limiting.

Thiele (*1*), Zeldovich (*2*), Wheeler (*3*), Aris (*4*), and others (*5–8*) have elaborated the theory of pore-diffusion-controlled reactions. The concentration gradients required to transport reactants into the reaction zone cause lowered concentration in the pellet interior. This results in a decreased reaction rate. The quantitative measure of the influence of this pore diffusion is given, for first order reaction, by the equation (all symbols defined in nomenclature section at end of article):

$$f = \frac{1}{\phi}\left[\frac{1}{\tanh 3\phi} - \frac{1}{3\phi}\right] \qquad (1)$$

where

$$\phi = \tfrac{1}{3}a(\sigma_s k/D'_e)^{1/2}$$

The effectiveness factor, f, is numerically equal to the ratio of reaction rate under pore-diffusion-controlled conditions to that which would occur if the concentrations of reactants throughout the granule were equal to that at the exterior surface. (External diffusion is not considered here.) The effectiveness factor, f, is a unique function of effectiveness factor modulus, ϕ, which in turn depends on effective diffusivity of the gases in the catalyst granule, D'_e.

Effective diffusivity also plays an important role in determining the maximum temperature in a catalyst granule (*9*), in calculating the effectiveness factor from a single measurement of conversion in an integral reactor (*10*) and in the kinetics of reactions in fixed beds (*11*).

Catalytic materials are produced either from porous powder particles which are pressed, extruded or tabletted into cylinders (designated here as "pellets"), or in the form of calcined gel spheres. The pore characteristics of these materials (designated here as "spheres") differ considerably in that spheres do not usually contain the extensive macropore structure of the pellets. This

micro-macrostructure arrangement has been discussed in more detail by Carberry (*12*).

The purpose of this paper is to present a method for measurement of gas diffusion rates in the microscopic matrix of porous spheres.

Review of Previous Experimental Techniques

One of the earliest methods of measuring gas diffusion in porous catalysts was developed by Graue (*13*) on the basis of the Hahn emanation technique (*14*). Catalyst structure was studied by measurement of the rate of movement of radioactive gas in the granules. Changes in the diffusion rate in ferric oxide materials were detected as a function of pretreatment temperature and addition of alumina.

The porous diaphragm cell, developed by Northrop and Anson (*15*, *16*), measures the nonsteady fluid diffusion rate between two well-mixed chambers separated by a porous cylindrical disc.

A more recent development of Mysels and Stigter (*17*) makes use of the principle of the porous diaphragm cell, but eliminates stirring problems through the use of two porous discs saturated with liquids.

Bolt and Innes (*18*) determined the effective diffusion rate of CO_2 in coal by continuously measuring the total gas evolved after releasing the pressure on an equilibrated sample. Reliable data could be obtained after about 30 sec from the beginning of the experiment.

Diffusion–sorption rates in molecular sieves were measured by Habgood (*19*) in a constant pressure flow system. After gas had flowed over the sieves for a desired length of time, the system was closed off and sorbed gases desorbed at high temperature. Data were obtained from about 1 min onward.

Catalyst effective diffusion coefficients have been measured indirectly from actual kinetic studies (*20*, *21*). Reaction rates at various conditions of internal diffusion were measured, yielding diffusivities from the effectiveness factor via the effectiveness factor modulus (*22*).

Liquid diffusion in catalysts has been measured by Baillie (*23*) from scintillation counter analyses of nonsteady elution by untagged *n*-hexane of a catalyst sample initially saturated with radioactive tritiated *n*-hexane.

The time-lag method of Barrer (*24*) has been frequently used in diffusion measurements in the free molecule flow regime. ("Flow" and "diffusion" are phenomenologically identical in this region.) Modifications for dead-end pore space have been considered by Goodknight and Fatt (*25*). The transient downstream pressure in a linear porous element is measured after application of a step function in pressure to the upstream end. The diffusivity is computed from the time-axis intercept of the extrapolated (steady state) portion of the downstream pressure vs. time curve. Winfield (*26*) measured transient sorption on catalyst materials in a constant volume system capable of yielding data in time periods of as small as 1 millisecond.

Determination of effective diffusivity by analogy from electrical measurements has been suggested by Wyllie and Rose (*27*) and subsequently confirmed experimentally (*28*). Fatt (*29*) found exact agreement between conductivity and diffusivity measurements using the method of Mysels and Stigter (*17*).

The most widely used experimental method for diffusivity measurement has been that of flow through a mounted porous element. Results of Rutz and Kammermeyer (*30*), Gilliland *et al.* (*31*), Arnell (*32*) and Urry (*33*) illustrate this technique, using a total pressure drop across cylindrical porous discs. Villet and Wilhelm (*34*) employed two different variations of this technique under unsteady conditions using the sphere mounting technique described in (*37*). Diffusivity measurements from flow at constant total pressure under a partial pressure gradient were first made by Wicke and Kallenbach (*35*), whose technique was modified by Weisz (*36*, *37*). Weisz (*37*) measured diffusivities by flow of hydrogen through spheres mounted by forcing them into undersized Tygon tubing (cf. ref. *37*, Fig. 1D). Experimental data taken on this arrangement, which produces diffusion in spherical geometry, are converted to diffusivities by

the application of a factor $\alpha = 0.78$ to the equation for purely linear flow.

General Description of the Method

The present technique consists of determining catalyst diffusivity from measurement of the transient release of hydrocarbon gas from the porous matrix of a sphere. The sphere is charged by exposure to a pure hydrocarbon gas for a sufficient time to allow the pores to fill by diffusion and for physical adsorption equilibrium to be reached. The hydrocarbon-containing pellet is then rapidly switched into a flowing stream of pure nitrogen, which flows over the surface of the sphere, eluting the hydrocarbon via a combined diffusion–desorption process (cf. ref. *38*, pp. 121–124). The hydrocarbon-containing nitrogen effluent stream then is mixed continuously with a flowing stream of pure hydrogen and fed to a hydrogen flame ionization detector. The signal resulting from the instantaneous hydrocarbon detection is continuously indicated on a potentiometric strip chart recorder. The effective diffusivity of the sphere is then computed from this continuous concentration–time plot.

Theory

The equations to be developed are those applying to diffusion accompanied by a nearly instantaneous physical desorption. The very rapid (compared to diffusion) rate of the physical sorption process has been demonstrated (cf. ref. *39*, pp. 4–19). Formulation of the differential equation for this process has been discussed by Crank (cf. ref. *38*, pp. 121–124). Under the assumption that the over-all diffusivity is constant and that the adsorption isotherm is linear, i.e.,

$$D'_e = \text{constant},\ \partial S/\partial t = R(\partial C'/\partial t),\quad R = (S_0/C'_0) \tag{2}$$

The boundary value problem is:

$$\begin{aligned} \partial\psi/\partial\tau &= \partial^2\psi/\partial x^2 \\ \psi(0, x) &= r \\ \psi(\tau, 0) &= \psi(\tau, \pi) = 0 \end{aligned} \tag{3}$$

Symbols and normalizations are specified in the nomenclature. The solution is

$$\frac{\psi}{r} = \frac{\bar{C}}{\bar{C}_0} = \frac{2}{x}\sum_{n=1}^{\infty}\frac{(-1)^{n+1}}{n}e^{-n^2\tau}\sin nx \tag{4}$$

from which

$$\left.\frac{\bar{C}}{\bar{C}_0}\right|_{\text{average}} = \frac{6}{\pi^2}\sum_{n=1}^{\infty}\frac{1}{n^2}e^{-n^2\tau} \tag{5}$$

The rate of hydrocarbon discharge, r_{He} (g mole/sec), from the spheres is:

$$r_{\text{He}} = \frac{-\partial\bar{C}_{\text{av}}}{\partial t}\left[\frac{4\pi a^3}{3}\right] = \frac{8C'_0D'_e\pi a}{\epsilon}\sum_{n=1}^{\infty}e^{-n^2\tau} \tag{6}$$

This discharging hydrocarbon is continuously mixed with nitrogen (flow rate V_{N} cc/sec), and hydrogen (flow rate V_{H} cc/sec) streams, and then fed to the flame ionization detector. The hydrocarbon concentration, C_s, in the gas stream flowing to the detector is thus:

$$C_s = \frac{r_{\text{He}}}{V_{\text{N}} + V_{\text{H}}} = \frac{8C'_0D'_e\pi a}{\epsilon(V_{\text{N}} + V_{\text{H}})}\sum_{n=1}^{\infty}e^{-n^2\tau} \tag{7}$$

Omitting terms in $n > 1$ gives the first order expression

$$\ln C_s = \ln\left[8C'_0D'_e\pi a/\epsilon(V_{\text{N}} + V_{\text{H}})\right] - \left[D'_e\pi^2/\epsilon(R + 1)a^2\right]t \tag{8}$$

In deriving Eq. (4), it is assumed that the transport rate in the pores is given by

$$q = -D'_eA(\partial C/\partial r) = -(D_e + D_s)A(\partial C/\partial r) \tag{9}$$

where D_e and D_s are the diffusivities for gas phase and surface transport, respectively. (It must be emphasized that these diffusivities do not involve ϵ as part of the definition.) The flux, q, is defined in terms of the total (fluid plus solid) area A normal to flow. The surface diffusivity is formally defined in terms of the gas phase concentration gradient by virtue of the instantaneous equilibrium existing between hydrocarbon in the gas phase and on the catalyst surface and the near-linearity of the adsorption isotherm. This formulation facilitates interpretation of results.

Equation (8) shows that an independent check on the value of D'_e may be obtained from a *single* experiment by comparison of the slope and intercept.

Apparatus and Experimental Technique

Equipment and Materials

Details of the diffusion cell are shown in Fig. 1. In operation, appropriately drilled N, D, and H, which are drilled and tapped for $\frac{1}{8}$-inch NPT. The diffusion cell is mounted directly under the flame ionization detector, the cell vent tube (F of Fig. 1) being connected to the base of the detector burner by approximately $1\frac{1}{2}$-inch of fine bore flexible Teflon tubing. The assembled unit is shown in Fig. 2. The diffusion cell is in the lower right, in test position, the hydrogen flame ionization detector above it ("FIAD" model,

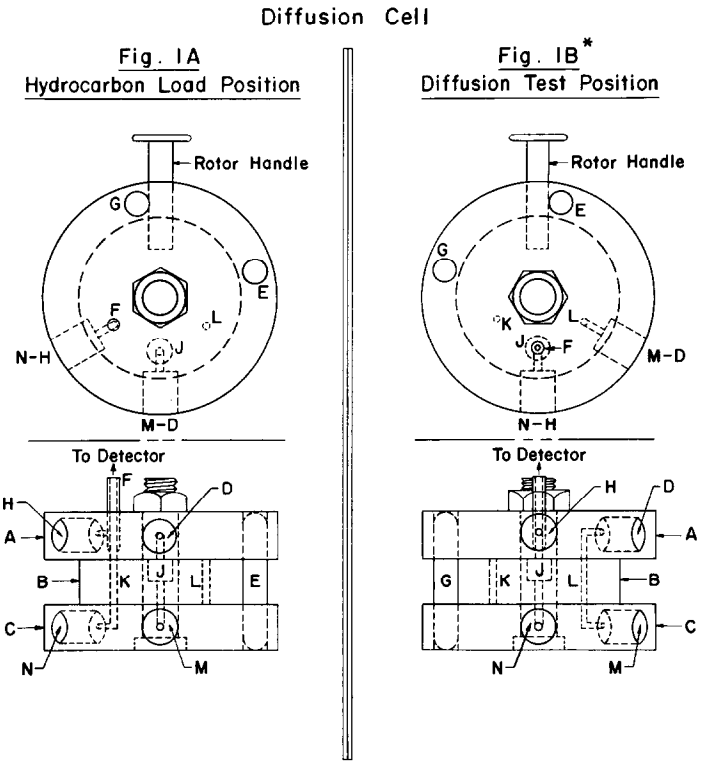

FIG. 1. *Diffusion Cell.* A, top plate—316 stainless steel; B, center plate (rotating)—316 stainless steel; C, bottom plate—316 stainless steel; D, hydrocarbon outlet; E, steel guide post; F, lead to detector; G, steel guide post; H, hydrogen inlet; I, tapped hole for rotor handle; J, catalyst chamber; K, valve port; L, valve port; M, hydrocarbon inlet; N, nitrogen inlet.

$\frac{1}{8}$-inch by $2\frac{1}{2}$-inch Teflon discs are inserted between A–B and B–C to give sealing and lubrication. The bolt and lock nut hold the three plates together with sufficient force to assure a leak-tight seal by the Teflon gaskets while allowing the central rotor to turn freely. Swagelok $\frac{1}{8}$-inch pipe to 1/16-inch tube connections fit into the chambers M, manufactured by Carad Corporation), the potentiometric recorder on the left (Varian Associates, model G-10, described in Varian Publ. No. 87-300-001), with an example of the pen-recorded raw data output from a typical diffusion experiment showing on its strip chart.

Characteristics of the five porous silica-

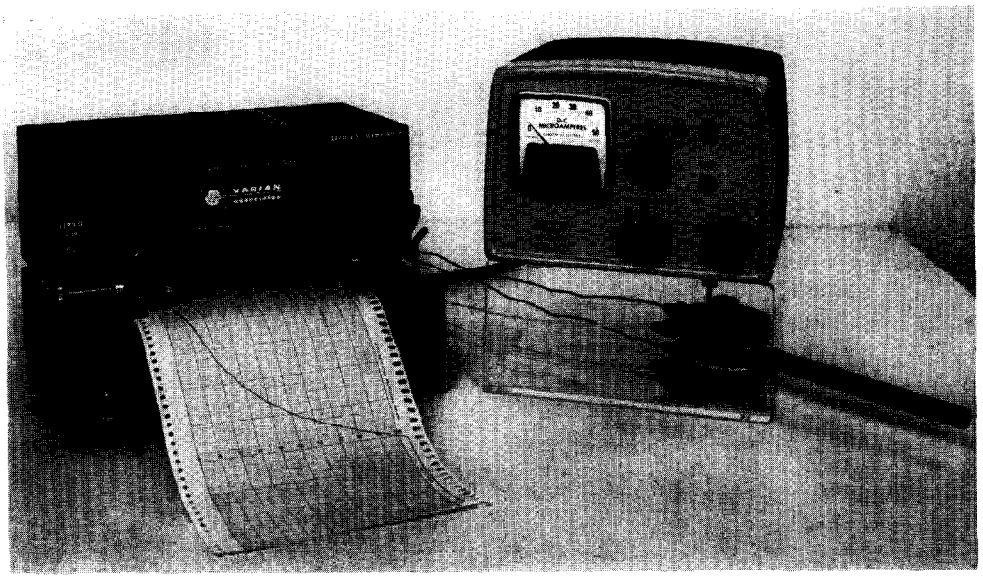

FIG. 2. Experimental setup showing cell (lower right), flame ionization detector above it, and potentiometric strip chart recorder at left with a portion of a raw data record.

alumina spheres used in the experiments are shown in Table 2. Phillips Research Grade methane, ethane, propane, and isobutane were used as the diffusing gases. All experiments were run at $22 \pm 1°C$ and 748 ± 5 mm Hg.

Experimental Technique

The general method has been described above (p. 343). With the cell in test position (Fig. 1B), the catalyst sphere in the cylindrical chamber, J, is purged by nitrogen. The nitrogen (about 80 cc/min entering at N) and hydrogen (about 100 cc/min entering at H) rates then are stabilized. The catalyst sphere is next switched into the hydrocarbon loading position (Fig. 1A) for a time sufficient to saturate the pore space completely. The saturating hydrocarbon gas enters at M (Fig. 1A) flows past the sphere in J, and leaves at D. The test experiment is performed by rapidly turning (in about 0.2 sec) the rotor element back to the test position, thus allowing the nitrogen stream to flow through the catalyst chamber, J, and over the sphere surface while the hydrocarbon stream is by-passed. During these operations, the detector burner is always lit and all flow rates remain constant. The hydrogen entering at H provides the burner fuel. Air is supplied externally. Gas residence time between the catalyst chamber and flame ionization burner tip was about 0.1 sec. Dispersion of the output in this connecting space was experimentally demonstrated to be negligible. This was done by increasing the elutant nitrogen rate to a level well above the point at which no further distortion of the diffusion output was observed.

Data may be taken at any convenient scale setting of the detector. The recorder must be operated at the maximum permissible ratio of signal to gain and with minimum damping. Minimum acceptable flow rates were found to be 1.50 cc/sec for hydrogen and 1.00 cc/sec for nitrogen. The catalyst sphere is protected from the direct impingement of the nitrogen stream by a thin aluminum foil disc placed on the floor of the catalyst chamber. All metal and Teflon contacting surfaces must be smooth and free from scoring or foreign matter. A small amount of spalling of the Teflon gaskets results after a number of cell rotations. Therefore, all contacting surfaces must be examined, wiped clean frequently, and repolished when necessary. Steel capillary tubing must be used for the hydrogen and

nitrogen leads to prevent random fluctuations in detector output.

Auxiliary Measurements

Catalyst spheres were outgassed under 0.1–0.5 micron pressure at 150–200°C for 5–10 hr, weighed to 0.0001 g, and measured to 0.001 inch. Skeletal densities of all materials were measured on a Beckman Model 930 Air Pycnometer. Surface area and pore-size distributions were determined by BET nitrogen adsorption and mercury porosimetry.

The extent of hydrocarbon adsorption on a given catalyst was measured using the technique described in "Experimental Technique," except that a vessel of approximately 200 cc volume was inserted between the cell vent tube, F, and the detector-burner. This arrangement was necessary because the normal diffusion test response has a very sharp peak—sufficient to send the recorder off-scale during the initial stages of elution. The additional capacity inserted spread out the hydrocarbon elution response to the point where the area of the resulting smooth curve could be measured by planimetry. This measurement gave M_T, the total number of moles of hydrocarbon adsorbed on the catalyst surface plus that contained in the pore volume and dead-space. The number of moles, M_C, contained in the empty cell was measured in the same way. These data, together with the measured skeletal volume of the sphere (equivalent to M_S moles), gave the quantity of hydrocarbon, M_0, adsorbed on the sphere at 1 atm as:

$$M_0 = M_T - M_C + M_S \qquad (10)$$

This determination was made for every run on each sample. The diffusion tests were performed immediately after the adsorption measurements without removing the sphere from the cell.

Dead-space response from the unoccupied portion of the catalyst chamber was measured by replacing the test sphere with a nonporous sphere of the same diameter. The dead-space in the cell was swept completely in 2 to 3 sec. Corrections (never more than 10% of total output) were made by subtracting the experimentally measured dead-space output from the diffusion test output. Detector response for all tests (diffusion, adsorption, and dead-space response) on each pellet–gas system was calibrated by substituting a nitrogen stream containing a known amount of hydrocarbon for the pure elutant nitrogen stream.

Adsorption isotherms were measured volumetrically between 0 and 1 atm at 22°C for all four gases on the materials of spheres No. 1 and No. 2 (see Table 2). These data were fitted by least squares to the linear form

$$S = E + RC' \qquad (11)$$

giving the percentage deviations shown in Table 1.

TABLE 1
PERCENTAGE DEVIATIONS FOR LINEAR FIT TO ADSORPTION ISOTHERMS

Gas	Sphere No. 1	Sphere No. 2
Methane	1.63	0.629
Ethane	5.92	3.00
Propane	7.53	5.36
i-Butane	18.3	17.7

The two sets of adsorption isotherms were measured under various total pressures of pure hydrocarbon while the actual diffusion experiments were made with a partial pressure of hydrocarbon in nitrogen. However, elementary considerations (cf. ref. *39*, pp. 85–87) show that the hydrocarbons adsorb as if the nitrogen were not present.

The surface characteristics of the spheres were not necessarily the same in the diffusion experiments as in the adsorption measurements. However, the *in situ* adsorption measurement [described in Eq. (10)], together with the assumption of linearity of the adsorption isotherms, allowed calculation of values of R [defined in Eq. (2)] which are listed in Table 2.

DATA ANALYSIS AND CALCULATION PROCEDURE

An example of the raw diffusion data is shown in Fig. 2. The beginning of the full-scale response to the step-function input imposed by switching gave an accurate and automatic indication of the "zero time."

TABLE 2

EXPERIMENTAL DATA FOR EFFECTIVE DIFFUSIVITIES OF SILICA-ALUMINA COMPOSITES

Diffusing gas	Sphere number	Composition (% Silica)[a]	Sphere Dia.[b] (cm)	Particle density, ρ (g/cm³)	Sphere porosity ϵ	Adsorption coefficient[c] R	Surface area (m²/g)	Avg. pore dia. (Å)	Dia. of largest pore (Å)	Effective diffusivity D'_e (cm²/sec)		Effective diffusivity, calc. from Eq. 15 (cm²/sec)	Surface diffusivity, $D_s = D'_e - D_e$ (cm²/sec)
										From slope	From intercept		
Methane	1	96	0.389	1.13	0.462	2.14	602	30.1	65.0	0.000508	0.000519	0.000508	—
Ethane	1	96	0.389	1.13	0.462	11.3	602	30.1	65.0	0.000597	0.000616	0.000371	0.000226
Propane	1	96	0.389	1.13	0.462	40.7	602	30.1	65.0	0.000883	0.000744	0.000306	0.000577
i-Butane	1	96	0.389	1.13	0.462	105	602	30.1	65.0	0.00117	0.00106	0.000266	0.000904
Methane	2	0	0.704	1.07	0.685	0.549	158	85.7	150	0.00576	0.00593	0.00576	—
Ethane	2	0	0.704	1.07	0.685	1.82	158	85.7	150	0.00450	0.00476	0.00420	0.00030
Propane	2	0	0.704	1.07	0.685	4.93	158	85.7	150	0.00364	0.00373	0.00348	0.00016
i-Butane	2	0	0.704	1.07	0.685	11.6	158	85.7	150	0.00340	0.00456	0.00302	0.00038
Methane	3	100	0.295	0.932	0.559	1.83	543	56.1	155	0.00194	0.00194	—	—
Methane	4	91.8	0.328	0.956	0.570	2.45	345	81.6	235	0.00396	0.00389	—	—
Methane	5	89.5	0.353	1.13	0.509	1.61	299	66.2	145	0.00143	0.00150	—	—

[a] Remainder alumina.

[b] Volume equivalent spherical diameter for slightly oblate spheroids.

[c] Cf. Eq. (2).

This is shown at the extreme lower end of the strip chart in Fig. 2. Dead-space response (cf. preceding section, "Auxiliary Measurements") was of the same form but descended to the recorder baseline well before the diffusion output. After subtracting the dead-space response and calibrating the output, as described in the aforementioned section, data points were selected randomly along the first order portion of the curve [$n = 1$ in Eq. (7)]. These points were fitted to a function of the form of Eq. (8) by the method of least squares. Effective diffusivity was independently computed from these least-squares-determined values of the slope B and intercept I by the equations:

$$D'_e = B\epsilon(R + 1)a^2/\pi^2 \qquad (12)$$

and

$$D'_e = \frac{I\epsilon(V_N + V_H)}{8C'_0\pi a} \qquad (13)$$

Porosity, ϵ, of each sphere was determined from its measured skeletal density, ρ_s, and particle density, ρ_a, from the relation:

$$\epsilon = 1 - (\rho_a/\rho_s) \qquad (14)$$

Results and Discussion

Cell effluent concentration–time curves (C_s vs. t) for four gases diffusing from sphere No. 1 are shown in Fig. 3. The solid lines were derived from Eq. (7). Least squares value of the slope and intercept were computed to fit the first order portion of the curves.* These values were used to calculate the higher order terms ($n > 1$) in Eq. (7). The arrows on Fig. 3 show the time beyond which the higher order effects contribute insignificantly to the total. This point has been arbitrarily chosen at $\tau = 5/3$.

Diffusivities calculated from similar curves

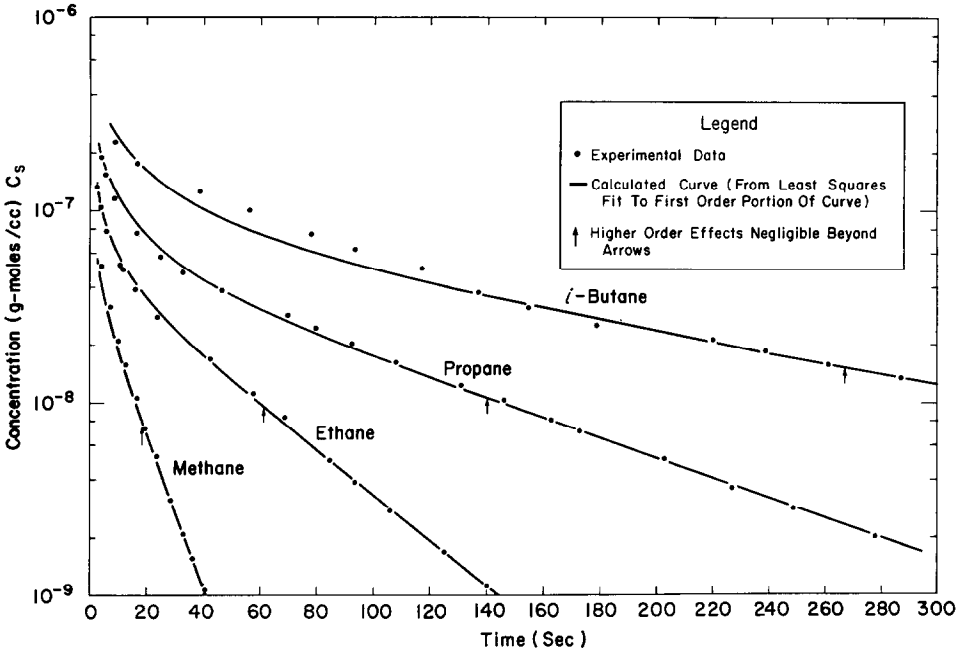

FIG. 3. Hydrocarbon concentration in effluent from diffusion cell vs. time from beginning of experiment for various gases diffusing from sphere No. 1. ●, *Experimental data;* —, *calculated curve* (from least squares fit to first order portion of curve). Higher order ($n > 1$) effects are negligible beyond the arrows. Propane and *i*-butane points beyond 300 sec have been omitted. Hydrogen rate = 1.50 cc/sec; nitrogen rate = 0.940 cc/sec.

* Omission of points for propane and isobutane beyond 300 sec from Fig. 3 was necessary because of space limitation. However, the omitted points were used in the least squares fit.

are shown in Table 2, together with all auxiliary data. The average percentage deviation from their respective least squares curves was 2.29% for the 123 data points in the 11 runs reported, taken from the first order sections of the curves.

An average percentage deviation of 2.25% was found for the effective diffusivities calculated from the intercept as compared with those calculated from the slope. Propane and isobutane runs are excluded because of the probable influence of concentration-dependent surface diffusion and deviation of the adsorption isotherms from linearity.

Examination of the data for diameter of largest pore shows that Knudsen diffusion was the prevailing mode of transport for all sphere–gas combinations. Under conditions of pure Knudsen diffusion, kinetic theory predicts that, for the same catalyst sphere, the diffusivity should be inversely proportional to the square root of the molecular weight of the diffusing gas. Table 2 shows that this is essentially true for sphere No. 2, but is not at all the case for sphere No. 1. The measured effective diffusivities for sphere No. 1 lie higher than those calculated from the square root relationship. The difference is attributed to surface diffusion, which leads to an increase in over-all diffusivity with increasing molecular weight of diffusing gas. These surface diffusivities [defined in Eq. (9)] have been computed using Eq. (15) for the C_2–C_4 hydrocarbons, as shown in the last column of Table 2. It was assumed that methane was transported by pure Knudsen diffusion. Methane diffusivities calculated from the slope were used for $D_{e,M}$ in all cases.

$$D_{s,i} = D'_{e,i} - D_{e,i} = D'_{e,i} - D_{e,M}(16.0/M_i)^{1/2} \quad (15)$$

(Subscript, i, refers to carbon number of diffusing hydrocarbons.)

Equation 5, describing the combined diffusion desorption process, also holds for an instantaneous reaction limited by diffusion (cf. ref. *38*, pp. 121–124). Although the theory has been known, experimental confirmation does not appear to have been disclosed. The data of Table 2 and Fig. 3 supply such confirmation. This is based on the following facts

1. The D'_e values determined from the first order section of the curves predict the behavior when higher order effects are important, as shown in Fig. 3.

2. The diffusivities computed from the slopes agree with those computed from the intercepts.

The latter holds true in spite of the profound influence of adsorption, reflected in the coefficient, R, on the slopes of the curves. This agreement cannot be fortuitous since the intercepts which do not contain R remain relatively constant for a given sphere, while the slopes vary over more than an order of magnitude for various diffusing gases.

The two major sources of disagreement between theory and data are deviation of the adsorption isotherm from linearity, and concentration dependence of surface diffusion coefficient. Qualitatively, the effect of these factors is seen to be virtually nil in the case of methane and ethane, small in the case of propane, and moderately large for isobutane.

The assumptions involved in derivation of the theory are most nearly satisfied when methane is used as a diffusing gas. In fact, measured isotherms were exactly linear in the range of 0 to 1 atm at 22°C for a wide variety of catalyst materials in addition to those reported here. Methane, therefore, is recommended for diffusion tests. However, for smaller-sized materials, ethane can be employed for purposes of obtaining better resolution between dead-space and diffusion response. The limit of accuracy of the apparatus was 10^{-10} moles/cc (as methane) at the flow rates used. Use of the present technique is, however, not limited to flame ionization detection and potentiometric recording. Any detector–recorder system suitable to the desired application may be used.

The method can be easily extended to the measurement of cylindrical pellets by the application of known mathematical techniques (cf. ref. *40*, pp. 225–229).

Average diffusivity of a number of spheres can be measured from a single experiment

using the technique reported here. Demonstration of this is given in the Appendix.

Nomenclature

a	Radius of sphere (cm)
A	Total cross-sectional area normal to flux of diffusing hydrocarbon (cm^2)
B	$D'_e\pi^2/\epsilon(R+1)a^2$ = slope of C_s vs. t curve
C	Concentration of hydrocarbon in gas phase (g moles/cc)
C'	Moles of hydrocarbon in void space of catalyst per unit volume of catalyst = ϵC (g moles/cc)
$\bar{C}$	$C' + S$
$\bar{C}_0$	$C'_0 + S_0$ (g moles/cc)
C'_0	Value at $t = 0$
C_s	Hydrocarbon concentration in feed to detector (g moles/cc)
D'_e	Over-all effective diffusivity (cm^2/sec)—defined in Eq. (9)
D_e	Effective diffusivity for gas phase transport (cm^2/sec)
$D_{e,M}$	Effective diffusivity for gas phase transport for methane (cm^2/sec)
D_s	Effective diffusivity for surface transport (cm^2/sec)
f	Effectiveness factor
I	$8C'_0D'_e\pi a/\epsilon(V_N + V_H)$ = Intercept of C_s vs. t curve (first order portion)
k	First order reaction rate constant (sec^{-1})
m	Number of spheres in sample
M_i	Molecular weight of hydrocarbon of carbon number, i
r	Distance from center of sphere (cm)
r_{Hc}	Rate of hydrocarbon discharge (g moles/sec)
R	Adsorption coefficient—defined in Eq. (2)
S	Moles of hydrocarbon adsorbed on catalyst surface per unit volume of catalyst, solid plus void (moles/cc)
S_0	Value at $t = 0$
t	Time (sec)
V_H, V_N	Volumetric flow rates of hydrogen and nitrogen (cc/sec)
x	$\pi r/a$
ϵ	Fraction voids
ρ_a	Particle density (g/cc)
ρ_s	Skeletal density (g/cc)
σ_s	Specific surface area (m^2/g)
τ	$D'_e\pi^2t/\epsilon(R+1)a^2$
ϕ	Effectiveness factor modulus—see Eq. (1)
ψ	$r(\bar{C}/\bar{C}_0)$

APPENDIX

Theory of Average Diffusivity for Multiparticle Systems

In measuring the diffusional properties of catalyst materials, the question of the average effective diffusivity of a batch of spheres having varying properties naturally arises. That the single-particle measurement technique previously described can actually be used for a multiparticle system will now be proven via theoretical generalizations from the basic theory.

We assume (subject to later verification) that only first order effects are of importance [Eq. (8)]. The hydrocarbon concentration being detected is, then, the sum of the contributions from all the spheres

$$C_s = \sum_{i=1}^{m} I_i e^{-B_i t} \tag{16}$$

where subscript, i, denotes the ith sphere in the batch of m spheres.

Define the mean value of the slopes B_i and intercepts I_i by

$$\bar{B} = \frac{1}{m}\sum_{i=1}^{m} B_i \quad \text{and} \quad \bar{I} = \frac{1}{m}\sum_{i=1}^{m} I_i \tag{17}$$

and the deviations of these values for the ith sphere from the mean by

$$\Delta B_i = P_i - \bar{B} \quad \text{and} \quad \Delta I_i = I_i - \bar{I} \tag{18}$$

Note also that, from the definition of the mean

$$\sum_{i=1}^{m} \Delta B_i = 0 \quad \text{and} \quad \sum_{i=1}^{m} \Delta I_i = 0 \tag{19}$$

Substituting for B_i from Eq. (18) into Eq. (16)

$$C_s = \sum_{i=1}^{m} (\bar{I} + \Delta I_i) \exp - (\bar{B} + \Delta B_i)t \tag{20}$$

Examination of Eq. (16) shows that, given enough time from the beginning of the experiment, the contribution to C_s of the sphere with the smallest value of slope B_i will eventually predominate over all the others. However, we are seeking to prove that valid experimental data can be obtained before the distortion due to this tendency becomes of serious concern.

The output from m uniform spheres, all having exactly the mean value of I and B is:

$$C_s{}^m = m\bar{I}e^{-\bar{B}t} \tag{21}$$

As long as $C_s/C_s{}^m$ remains close to unity the actual batch of m spheres of varying properties approximates the behavior of the m uniform spheres.

$$C_s/C_s{}^m = (1/mIe^{-\bar{B}t}) \sum_{i=1}^{m} (\bar{I} + \Delta I_i) \exp - (\bar{B} + \Delta B_i)t \tag{22}$$

It is recognized that the time-dependent term is the critical factor and neglect of the ΔI_i is a reasonable first order approximation. Equation (21), after some manipulation and series expansion, becomes

$$\frac{C_s}{C_s{}^m} = 1 - \sum_{i=1}^{m} \frac{\Delta B_i t}{m} + \sum_{i=1}^{m} \frac{\overline{\Delta B_i t}^2}{2!m} + \ldots + \sum_{i=1}^{m} (-1)^n \frac{\overline{\Delta B_i t}^n}{n!m} \tag{23}$$

Truncation of the series after the quadratic term, use of Eq. (19), definition of the standard deviation of the values of B_i from their mean, and solution gives:

$$(C_s/C_s{}^m) - 1 = (m - 1)\sigma^2 t^2/2m \tag{24}$$

As an example, the largest slopes, B, observed for the experimental data reported in Table 2 were about 0.5 sec^{-1}. Assume a hypothetical batch of 10 pellets whose standard deviation is $\sigma = 0.1\bar{B} = 0.05$, and that 10% maximum error in the approximation can be accepted, i.e.,

$$[(C_s/C_s{}^m) - 1]_{max} = 0.10$$

Then the time within which this approximation error is 10% or less is 9.41 sec. Since higher order effects can be shown to be negligible beyond about 3 sec, there is a definite time range within which the output from the multiparticle system reflects the true mean diffusivity. Data output in this time range can be easily handled by the apparatus.

References

1. Thiele, E. W., *Ind. Eng. Chem.* **31**, 916 (1939).
2. Zeldovich, Y. B., *Acta Physicochim. URSS* **10**, 583 (1939).
3. Wheeler, A., *Advan. Catalysis* **3**, 250 (1951).
4. Aris, R., *Chem. Eng. Sci.* **6**, 262 (1957).
5. Pomerantsev, V. V., *Inzk.-Fiz. Zh., Akad. Nauk Belorussk.* SSR **2**, 3 (1962).
6. Adelson, S. V., and Zaitova, A. Ya., *Khim i Tekhnol Topliva i Masel* **1**, 25 (1962).
7. Kubota, H., Shindo, M., Akehata, T., and Lin, E., *Kagaku Kogaku* **23**, 284 (1959).
8. Pannetier, G., *Bull. Soc. Chem., France,* pp. 2126 and 2131 (1961).
9. Damköhler, G., *Z. Physik. Chem.* **A193**, 16 (1943).
10. Wagner, C., *Z. Physik. Chem.* **A193**, 1 (1943).
11. Smith, N. L., and Amundson, N. R., *Ind. Eng. Chem.* **43**, 2156 (1951).
12. Carberry, J. J., *A.I.Ch.E.J.* **8**, 557 (1962).
13. Graue, G., and Koch, H. W., *Chem. Ber.* **73B**, 984 (1940).
14. Hahn, O., *Naturwissenschaften* **17**, 295 (1929).
15. Northrop, J. H., and Anson, M. L., *J. Gen. Physiol.* **12**, 543 (1929).
16. Gordon, A. R., *Ann. N. Y. Acad. Sci.* **46**, 285 (1945).
17. Mysels, K. J., and Stigter, D., *J. Phys. Chem.* **57**, 104 (1953).
18. Bolt, B. A., and Innes, J. A., *Fuel* **38**, 333 (1959).
19. Habgood, H. W., *Can. J. Chem.* **36**, 1384 (1958).
20. Sokolova, D. F., *Zh. Fiz. Khim.* **33**, 471 (1959).
21. Wicke, E., and Brötz, W., *Chem.-Ingr.-Tech.* **21**, 219 and 319 (1949).
22. Hoogschagen, J., *Ind. Eng. Chem.* **47**, 906 (1955).
23. Baillie, L. A., paper presented at *Catalyst Club of Chicago Symposium, Northwestern University, April 14, 1962.*
24. Barrer, R. M., and Barrie, J. A., *Proc. Roy. Soc. (London)* **A213**, 250 (1952).

25. GOODKNIGHT, R. C., AND FATT, I., *J. Phys. Chem.* **64,** 1162 (1960); **65,** 1709 (1961); and **66,** 760 (1962).
26. WINFIELD, M. E., *Australian J. Chem.* **6,** 221 (1953).
27. WYLLIE, M. R. J., AND ROSE, W., *Nature* **165,** 972 (1950).
28. SCHOFIELD, R. K., AND DAKSHINAMURTI, C., *Disc. Faraday Soc.* **3,** 56 (1948).
29. FATT, I., *J. Phys. Chem.* **63,** 751 (1959).
30. RUTZ, L. O., AND KAMMERMEYER, K., *U. S. Atomic Energy Comm.* **AECU-4328,** 54 (1959).
31. GILLILAND, E. R., AND BADDOUR, R. F., *A.I.Ch.E.J.* **4,** 90 (1959).
32. ARNELL, J. C., *Can. J. Res.* **A24,** 103 (1946); **A25,** 191 (1947).
33. URRY, W. D., *J. Am. Chem. Soc.* **55,** 3242 (1933).
34. VILLET, R. H., AND WILHELM, R. H., *Ind. Eng. Chem.* **53,** 837 (1961).
35. WICKE, E., AND KALLENBACH, R., *Kolloid-Z.* **97,** 135 (1941).
36. WEISZ, P. B., AND SCHWARTZ, A. B., *J. Catalysis* **1,** 399 (1962).
37. WEISZ, P. B., *Z. Physik. Chem.* (*Frankfurt*) **11,** 1 (1957).
38. CRANK, J., "The Mathematics of Diffusion." Oxford, Clarendon Press, 1956.
39. DEBOER, J. H., "The Dynamical Character of Adsorption." Oxford, Clarendon Press, 1953.
40. CARSLAW, H. S., AND JAEGER, J. C., "Conduction of Heat in Solids," 2nd ed. Oxford, Clarendon Press, 1959.